THE JOURNAL OF THE ACOUSTICAL SOCIETY OF KOREA Vol.29, No.1E, 2010. 3, pp. 1~10

Ultrasound Elasticity Imaging Methods

Mok-Kun Jeong* and Sung-Jae Kwon*
*Departments of Electronic and Communication Engineering, Daejin University
(Received February 5, 2010; accepted March 9, 2010)

Abstract

The difference in echogenicity between cancerous and normal tissues is not quite distinguishable in ultrasound B-mode imaging. However, tumor or cancer in breast or prostate tends to be stiffer than the surrounding normal tissue. Thus, imaging the stiffness contrast between the two different tissue types is helpful for quantitative diagnosis, and such a method of imaging the elasticity of human tissue is collectively referred to as ultrasound elasticity imaging. Recently, elasticity imaging has established itself as an effective diagnostic modality in addition to ultrasound B-mode imaging. The purpose of this paper is to present various elasticity imaging methods that have been reported up to now and to describe their principles of operation and characteristics.

Keywords: *ARFI, Elastography, SSI, Sonoelastography, SWEI, Vibro-acoustography*

I. Introduction

The image resolution of diagnostic ultrasound scanners has increased significantly with advances in semiconductor technology. Ultrasound B-mode imaging is based on the amplitude of reflected echoes arising from acoustic impedance differences in a medium, and displays the anatomical structure. However, cancer in soft tissue usually does not have a clear boundary with the surrounding tissue, and cannot be differentiated in ultrasound B-mode image. Therefore, over the past several decades, many research efforts have been made to measure intrinsic tissue parameters of normal and cancerous tissues, such as the speed of sound, attenuation coefficient, nonlinear parameter, elasticity, etc. [1-5].

It is worth noting that two imaging modalities have been commercialized. One is harmonic imaging that utilizes nonlinear effects that occur during ultrasound propagation, and the other is elasticity imaging that visualizes the stiffness distribution of tissue by measuring the hardness of cancerous tissue relative to its surrounding tissue and presenting it as an image.

Palpation examines tissue hardness by means of manual compression, and has traditionally been used as a handy method of diagnosing cancer that lies close to human skin. However, because it depends on the skill and experience of an operator, much research has been going on to find a more reliable and objective ultrasound diagnostic method.

A group led by Ophir [5] is the first to successfully demonstrate the feasibility of imaging the elasticity distribution of a medium. They produced strain images while applying compression.

The principle of obtaining strain image by applying compression is shown in Fig. 1. If an object consisting of hard and soft media is subjected to compression, the soft medium will deform more than the hard media. In order to obtain strain ϵ, we first find the amount of displacement at tissue positions, and then differentiate it to determine the relative

Corresponding author: Mok-Kun Jeong (jmk@daejin.ac.kr)
Department of Electronic Engineering, Daejin University, Pocheon, Gyeonggi 487-711, Korea

rate of change in displacement. The Young's modulus is defined as

$$E = \frac{\sigma}{\epsilon}, \tag{1}$$

where σ denotes the applied stress. Accordingly, elasticity imaging is a method of imaging the Young's modulus of an object, but in reality, since the distribution of the stress is difficult to determine, methods of imaging only the strain distribution have reached the commercialization stage.

Ultrasound elasticity imaging can be used to diagnose soft tissue malignancies related to breast, prostate, thyroid, blood vessel, and OB/GYN. The elastic moduli of cancerous breast and prostate tissues are more than three times larger than their normal counterparts, and tend to increase with increasing stress, exhibiting their nonlinear characteristics [6].

Techniques for elasticity imaging can be categorized by the type of applied stress. Table 1 lists various methods of imaging tissue elasticity that are classified according to the type and frequency of stress source.

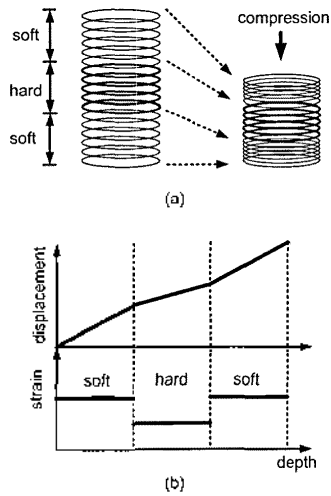

Fig. 1. Principle of measuring strain by applying compression to tissue: (a) displacement varying with tissue stiffness and (b) displacement and strain profiles with depth.

Now we will look into the principles and characteristics of various elastic imaging methods.

II. Displacement Estimation in Strain Imaging

Strain imaging first finds the amount of displacement that scatterers undergo as the deformation is applied to them, and differentiates it to determine the strain. Strain imaging is also known as freehand, or quasi-static, compression elastography. The amount of displacement in a medium varies with its strain distribution whose estimation is the main purpose of strain imaging. The most important signal processing operations in strain imaging are the displacement estimation and suppression of noise arising from differentiation of the displacement.

To obtain strain image with quasi-static compression technique, the acquisition of ultrasound data proceeds as follows. First, an ultrasound reference signal is acquired from an object before applying compression, and another ultrasound signal is acquired from the same object after applying compression. When the object is compressed, the scatterers inside it move in the direction of compression, making the echo arrival times shifted in time relative to those before applying compression. Thus, the displacements of the scatterers can be found by estimating the amount of time shift between the pre- and post-compression echoes. These displacements vary with the object stiffness, and thus are representative of the object characteristics. They can be computed from radio

Table 1. Classification of elasticity imaging methods by stress source and frequency.

Stress Frequency	Stress Source	Method
Less than 5 Hz	Manual palpation	Strain imaging
Sine wave of tens to hundreds of Hz	Mechanical vibration	Sonelastography
	Acoustical vibration	Vibro-acoustography
Impulse	Mechanical impulse	Transient elastography
	Acoustical radiation force	ARFI imaging Supersonic imaging

frequency (RF) or complex baseband echo signals using autocorrelation, crosscorrelation, or speckle tracking methods. In order to enable real time implementation, fast algorithms are required considering the large amount of ultrasound image data. The speckle tracking method, the iterative phase zero root seeking method, and the combined autocorrelation method can compute displacements fast from the phase difference of complex baseband signals [7–9].

Next, we introduce a method of estimating displacement using autocorrelation [10]. Ultrasound RF data are first demodulated to the baseband to obtain both in-phase and quadrature components, which are then combined into a complex signal, referred to as complex baseband signal. Taking the autocorrelation of the pre- and post-compression complex baseband signals yields the phase difference, from which the time delay can be found. The compressed, i.e., time-delayed version of a signal can be modeled using an allpass filter. Denoting the pre- and post-compression signals as $y_1(t)$ and $y_2(t)$, respectively, we obtain the demodulated complex baseband signals as follows:

$$\begin{aligned} y_{1b}(t) &= r(t)e^{j\phi(t)}, \\ y_{2b}(t) &= r(t-\tau)e^{j(-w_0\tau+\phi(t-\tau))}, \end{aligned} \tag{2}$$

where $r(t)$ is the envelope, w_0 is the central angular frequency, τ is the time delay, and $\phi(t)$ is the phase of the complex baseband signal $y_{1b}(t)$. Following sampling, the phase difference between the two finite-duration sequences, $y_{1b}(n)$ and $y_{1b}(n)$, can be expressed as:

$$\Delta\Phi = \arg < y_{1b}(n) \cdot y_{2b}^{*}(n) > = w_0\tau + \phi(t) - \phi(t-\tau). \tag{3}$$

where arg denotes the phase, and the operation inside the brackets is the inner product to find the amount of correlation. Taking a Taylor series expansion of the phase term, $\phi(t-\tau)$, in (3) and keeping up to the linear term gives

$$\tau = \frac{\Delta\Phi}{w_0 + \phi'(t)} = \frac{\Delta\Phi}{w_0 + w_D(t)}, \tag{4}$$

where $w_D(t)$ equals the phase derivative, $\phi'(t)$, which corresponds to the instantaneous frequency of the complex baseband signal. The displacement is then computed from the phase difference. This method takes into account the variation of the center frequency with increasing depth, and requires fewer computations than crosscorrelation methods.

If displacement is estimated without considering the decorrelation between the pre- and post-compression signals, it is equivalent to just computing the phase difference between them over a finite interval. As the imaging depth increases, the displacement also increases and the decorrelation between them tends to increase. Thus, it is inevitable that displacement estimation errors increase. To overcome this problem, we first estimate δ, which is the delay between them, shift the post compression signal against the pre-compression signal, and then estimate the remaining displacement. The amount of displacement estimated in the previous data window is used as the value of δ. The post-compression complex baseband signal, which has been shifted in the direction of decreasing phase difference, is given by

$$y_{2b}(t+\delta) = r(t-\tau+\delta)e^{j(-w_0\tau+\phi(t-\tau+\delta))}. \tag{5}$$

The phase difference between the pre- and post-compression signals is expressed as

$$\Delta\Phi_\delta = \arg[< y_{1b}(n) \cdot y_{2b}^{*}(n+\delta) > \cdot e^{j(-w_0\delta)}]. \tag{6}$$

The time delay is estimated as

$$\tau = \frac{\Delta\Phi_\delta}{w_0 + \phi'(t)} + \delta. \tag{7}$$

This two-step method is generally used for strain estimation [9,10]. In the method, the phase difference

between the two signals is estimated first and used in reducing the phase difference, and then the final displacement is estimated again.

Fig. 2 shows the distribution of strain inside a plastic phantom embedded with two 10-mm diameter and one 20-mm diameter hard cylinders in the soft background, which is subjected to a strain of 0.2%. The cylinders are about five times harder than the background. The top panel of Fig. 2 shows an ultrasound B-mode image where the boundaries of the cylinders can be discerned but the speckle patterns of the cylinders and the background look similar. In general, finding cancer is difficult because the boundary between the cancer and the surrounding normal tissue is not quite clear. The middle panel of Fig. 2 shows an image of the displacement along the direction in which the compression is applied. The bottom panel of Fig. 2 represents an image of the strain, and is obtained by differentiating the displacement along the direction in which the compression is applied. It can be seen that the strain image has a higher contrast than its corresponding B-mode image counterpart.

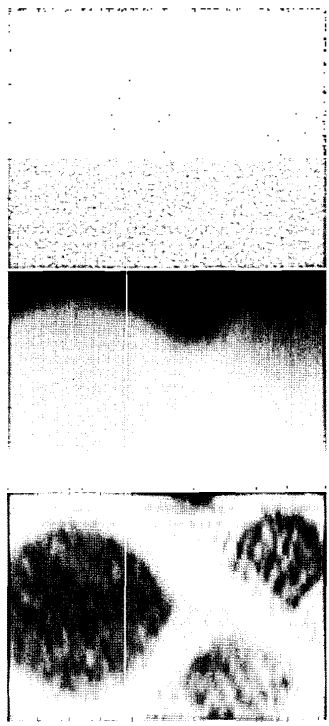

Fig. 2. Comparison of phantom images: B-mode (top), displacement (middle), and strain (bottom).

Fig. 3 compares displacement estimates obtained using the crosscorrelation method (solid line) and the autocorrelation method of (7) with (dotted line) and without (dashed line) compensating for the variation of $\omega_0(t)$. The algorithms were applied to the scan line data that passed through the center of the larger cylinder whose diameter is 20 mm. The crosscorrelation method was performed after resampling the RF data at 2.094 GHz. The result can be considered as a gold standard because the errors are very small. For the case that the displacement was estimated using the autocorrelation method, compensation of the center frequency variation results in an estimation performance similar to the crosscorrelation method. In practice, however, the autocorrelation method may incur significant errors due to signal decorrelation and speckle noise. The decorrelation is attributed to lateral and out-of-plane motions. To obtain more accurate displacement estimates, techniques such as signal stretching, linear regression based differentiation, persistence processing were proposed [11-15].

The Ophir group [16-18] actively reported

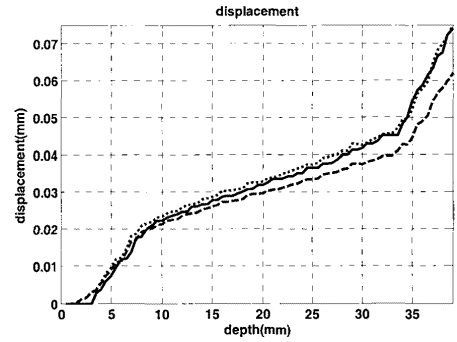

Fig. 3. Comparison of displacements estimated using cross-correlation (solid) and autocorrelation with (dotted) and without (dashed) center frequency correction.

clinical test results to demonstrate the efficacy of strain imaging techniques. The left and right panels of Fig. 29 of Ref. [18] compare the ultrasound B-mode and strain images of an invasive ductal carcinoma, respectively. The dark area in the strain image indicates that the lesion is stiff, and is marked by cross symbols for size comparison. The size of the lesion in the strain image is confirmed to be different from that in the B-mode image depending on whether it is benign or malignant. This finding suggests that a significant reduction in the number of biopsies of benign lesions is possible using both elastography and sonography together [18].

III. Transient Elastography and Sonoelastography

The strain imaging method just introduced applies compression to a medium slowly so that the medium has enough time to respond to the compression. However, tissue elasticity can also be measured from the characteristics of stress propagation while applying a mechanical impulse in a short period of time or a mechanical harmonic motion for a long time.

The category of applying mechanical impulse includes transient elastography introduced by the Fink group [19,20]. If a mechanical impulse is applied to human tissue, a longitudinal wave propagates in the direction of the applied impulse, and also a shear wave is generated in the lateral direction. As the shear wave slowly propagates inside the human body, the movement of tissue is visualized by a high frame-rate imaging technique. The frame rate is as high as up to 6000 frames/s.

Another method is sonoelastography that applies a mechanical harmonic sinusoidal wave to the human body and measures the amount of vibration in the soft tissue due to the generated shear wave. At that time, all the tissue vibrates at the same frequency, and thus the soft part vibrates greater than the hard part. It is the sonoelastography technique that images the vibration amplitude of soft tissue using a Doppler method. The technique was investigated by the Parker group [21,22].

IV. Acoustic Radiation Force Impulse Imaging Technique

Stress is delivered to the human body using externally applied mechanical force, for example, quasi-static compression, transient mechanical impulse, mechanical harmonic oscillation, etc. The elasticity image quality of the above methods depends on the experience and skill of an ultrasonographer, and the use of a mechanical assembly or setup for consistent application of compression may complicate the data acquisition process.

To cope with this disadvantage, methods of generating acoustic radiation force and controlling the stress magnitude and the position where stress is generated as desired have been sought. These methods are intended to reduce displacement estimation errors by removing the operator's motion. The process of ultrasound image formation proceeds by transmitting a longitudinal wave that propagates into a tissue of interest while vibrating in the same direction and applies force to it. The force is termed acoustic radiation force. The following relationship holds:

$$F = \frac{W_{absorbed}}{c} = \frac{2\alpha I}{c}, \tag{8}$$

where F is the acoustical radiation force in $kg \cdot s^{-2} \cdot cm^{-2}$, α is the attenuation coefficient in $Np \cdot m^{-1}$, $W_{absorbed}$ is the power absorbed by the medium at a given spatial location, c is the speed of sound in the medium in ms^{-1}, and I is the temporal average intensity at a spatial location in $W \cdot cm^{-2}$.

Elasticity imaging methods that utilize acoustic radiation force are divided into acoustic radiation force impulse (ARFI) and shear wave elasticity

imaging (SWEI).

When a high-intensity ultrasound wave is focused onto a small region in a short time, the focused tissue is pushed. The maximum shift that the tissue undergoes and the time it takes the tissue to return to its original position are inversely proportional to the tissue stiffness. Fig. 4 shows a focal depth where a radiation force and a shear wave are generated in the axial and lateral directions, respectively.

An elasticity imaging technique using this principle was introduced and termed ARFI imaging [23-31]. It transmits a localized high intensity impulsive ultrasound radiation force to an imaging region of interest and observes the resulting motion. Fig. 5

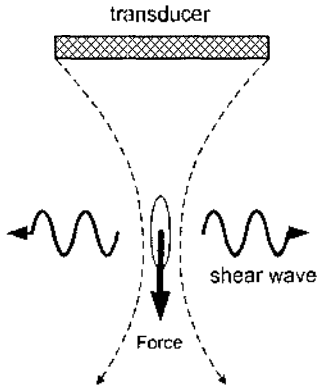

Fig. 4. Generation of radiation force and shear wave by transmission of high-intensity impulsive ultrasound wave.

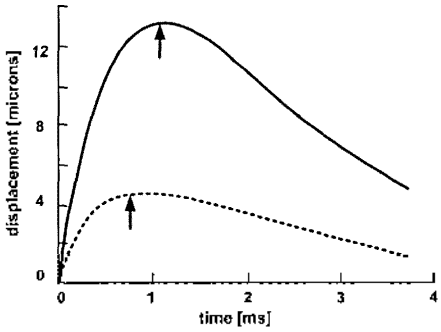

Fig. 5. Displacements of soft (solid) and hard (dotted) media due to high-intensity ultrasound wave where the arrows indicate the time to the peak displacement.

depicts the displacements in a medium at a focal point with time due to a high-intensity impulsive ultrasound wave [24]. The solid and dotted lines correspond to the hard and soft media, respectively. The arrows indicate the time to reach the maximum displacement. The amount of displacement and the time to reach the maximum displacement are larger in the soft medium than in the hard medium.

For a human breast with a palpable invasive ductal carcinoma, Fig. 6 shows the B-mode image (left), the maximum displacement image (center), and the time to the maximum displacement image (right) [27]. The characteristics in the lesion are displayed to be different from those in the background. The x and y axes in the images represent the lateral and axial directions, respectively. The transducer is located at the top of the images. Note a number of reversals in contrast between the two ARFI data images. Although the focal region of the pushing beams was 20 mm, it appears that a fairly uniform force field is applied from 5 to 20 mm in depth. This is expected due to the relatively high attenuation of breast tissue, which ranges from 1 to 3 $dB \cdot cm^{-1} \cdot MHz^{-1}$.

V. Vibro-Acoustography

If we generate harmonic oscillation using two signals of different frequencies, a beat phenomenon occurs in areas of tissue where the two signals overlap because the tissue is nonlinear. If two focused ultrasound continuous waves whose frequency difference is very small are transmitted using two transducers, a beat frequency signal is generated in a tissue area where the two transmit fields intersect, and the beat signal amplitude depends on the elasticity characteristics of the medium. Because the beat signal frequency is very low, it can be measured using a hydrophone. If the area over which ultrasound waves intersect is adjusted by focusing transmit ultrasound, a high resolution elasticity

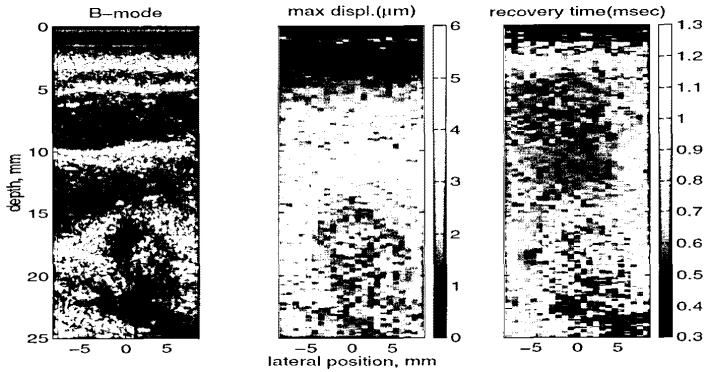

Fig. 6. *In vivo* human breast with palpable invasive ductal carcinoma: B-mode image (left), maximum displacement image (center), and recovery time image (right) [27].

image can be obtained. This elasticity imaging method was introduced by the Greenleaf team and termed vibro-acoustography [32-36].

Fig. 7 shows the principle of vibro-acoustography. The left and right panels of Fig. 5 of Ref. [36] represent X-ray and vibro-acoustography images of a mostly calcified human breast with fibroadenoma, when the ultrasound beam is focused at a depth of 4 cm from the skin. The lesion in the vibro-acoustography image can be seen clearly almost the same as in the X ray image, and appears black because the calcification is very dense.

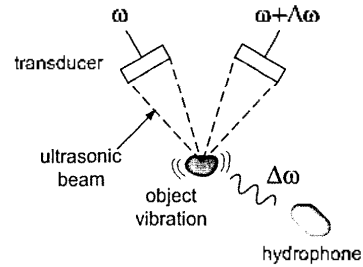

Fig. 7. Principle of the vibro-acoustography.

VI. Shear Wave Elasticity Imaging

Fig. 1 of Ref. [23] shows the range of shear and bulk modulus values for various human tissues. The bulk modulus of liquids, soft tissue, and bone is clustered in a narrow range from 10^9 Pa to 10^{10} Pa, while the shear modulus has a wide dynamic range from as small as 10^3 Pa for glandular tissue of breast, liver, relaxed muscle, and fat to as large as 10^{10} Pa for bone. The shear modulus of dermis, connective tissue, contracted muscle, and papable nodules ranges from 10^5 Pa to 10^6 Pa, and that of epidermis and cartilage is in the range between 10^7 Pa and 10^8 Pa [23]. It is evident that the shear modulus has a wider dynamic range than the bulk modulus. Thus, imaging the shear modulus offers more potential for quantitative diagnosis.

The aforementioned elasticity imaging methods apply stress mechanically or uses acoustic radiation force. Therefore, the force applied cannot be exactly determined, and the elasticity cannot be measured quantitatively. To overcome this disadvantage, methods of generating shear wave using acoustic radiation force and measuring the propagation speed of shear wave were reported, including shear wave elasticity imaging (SWEI) and supersonic imaging (SSI) techniques [23,37-40]. At the transmit focus, the axial vibration of a longitudinal wave generated by ARFI generates a shear wave in the lateral direction. The longitudinal wave propagates at a

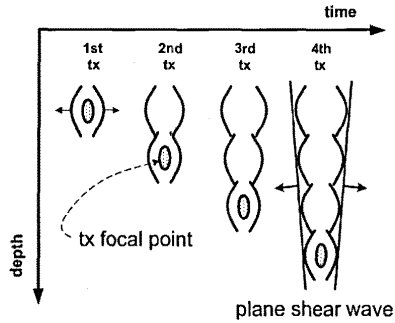

Fig. 8. Generation of the supersonic shear source where the source is sequentially moved along the beam axis, creating two plane- and intense-shear waves propagating in opposite directions.

speed of 1540 m/s, while the shear wave propagates very slowly at a speed of 1 to 10 m/s. The propagation speed of a shear wave depends on the shear modulus of a medium in which it travels, and is given by the following relationship:

$$C_L = \sqrt{\frac{\lambda + 2\mu}{\rho}} = \sqrt{\frac{(1-\nu)E}{(1+\nu)(1-2\nu)\rho}}, \qquad (9)$$
$$C_T = \sqrt{\frac{\mu}{\rho}} = \sqrt{\frac{E}{2(1+\nu)\rho}},$$

where λ is the elastic Lamé coefficients, ρ is the density of the material, μ is the material shear modulus, E is the Young's modulus, ν is the Poisson's ratio, and C_L and C_T are constants representing the longitudinal and transverse (shear) wave speeds, respectively. In soft media λ is 10^6 times bigger than μ and $\nu \approx 0.5$. Thus, a good approximation of E is given by

$$E \approx 3\mu. \qquad (10)$$

Therefore, if the propagation speed of a shear wave inside a medium is measured, its elasticity can be quantitatively determined. Also, because the shear elasticity has a wide dynamic range depending on media, it is better for lesion diagnosis to measure the shear modulus than bulk modulus.

Elasticity imaging techniques that directly measure shear modulus using the propagation speed of a shear wave are useful in monitoring the progress of lesion because it quantitatively determines the tissue elasticity. Many companies are making efforts to commercialize them, and a Siemens product is already available on the market which shows the propagation speed of a shear wave in lesion by combining with transient ARFI imaging [40]. The region where shear wave is generated in ARFI technique is limited to the vicinity of a transmit focal point. To construct an elasticity image over a large area requires a long data acquisition time. Supersonic imaging or shear wave elastography overcomes this problem by generating a plane shear wave using ARFI technique and measuring the propagation speed of shear wave in a medium, and thereby visualizes the shear modulus over the entire imaging area simultaneously [37-40].

A method of generating plane shear waves is shown in Fig. 8 [37]. The shear waves are generated near the transmit focal point. If the shear waves are transmitted multiple times while moving the focal depth in the axial direction, the wavefronts of the shear waves generated at individual focal points are superposed, and as a result the plane shear waves are generated. As the shear waves propagate inside a medium, the speed changes depending on the medium characteristics. A high frame rate system capable of imaging up to several thousand frames per second monitors the displacement of medium to estimate the propagation speed of the shear waves. Because it is possible to compute the shear or bulk modulus from the propagation speed of the shear wave, the medium elasticity can be determined quantitatively.

Fig. 6 of Ref. [38] compares the ultrasound B-mode (left) and supersonic shear (right) images of a human breast lesion. The shear wave speed is coded on a color scale of 0 to 9 m/s, which corresponds to the Young's modulus values ranging from 0 to 240 kPa). The case is a very small hypoechoic lesion classified as BI-RADS category 5. This small lesion whose diameter is 5 mm is rather

difficult to detect in the ultrasound B-mode image because its echogenicity is not significantly different from that of normal parenchyma. The elasticity map clearly delineates a small hard region with a Young's modulus of about 165 kPa. The margins are properly depicted with an average 5-mm diameter. The lesion size was confirmed after biopsy by a pathologist and the final diagnosis was an infiltrating ductal carcinoma grade III.

VII. Conclusion

Among tissue parameter imaging methods, elasticity imaging techniques have been relatively successfully developed, and find their applications in diagnostic ultrasound imaging as a new complementary modality. In particular, strain imaging techniques have been commercialized by several major companies and are now in clinical use. It is envisaged that in the near future elasticity imaging techniques will be a viable diagnostic ultrasound imaging modality with the advancement in understanding ultrasound physics and developing hardware technology.

References

1. T. Sato, Y. Yamakoshi, and T. Nakamura, "Nonlinear tissue imaging," in *Proc. IEEE Ultrason. Symp.*, 1986, pp. 889-900.
2. D. Yanwa, T. Jia, and S. Yongchen, "Relations between the acoustic nonlinearity parameter and sound speed and tissue composition," in *Proc. IEEE Ultrason. Symp.*, 1987, pp. 931-934.
3. P. He and A. McGoron, "Parameter estimation for nonlinear frequency dependent attenuation in soft tissue," *Ultrasound Med. Biol.*, vol. 15, no. 8, pp. 757-763, 1989.
4. Y. Hayakawa, T. Wagai, K. Yosioka, T. Inada, T. Suzuki, H. Yagami, and T. Fujii, "Measurement of ultrasound attenuation coefficient by a multifrequency echo technique—Theory and basic experiments," *IEEE Trans. Ultrason. Ferroelectr. Freq. Control*, vol. 33, no. 6, pp. 759-764, Nov. 1986.
5. J. Ophir, I. Cespedes, H. Ponnekanti, Y. Yazdi, and X. Li, "Elastography: A quantitative method for imaging the elasticity of biological tissues," *Ultrason. Imaging*, vol. 13, pp. 111-134, 1991.
6. T. A. Krouskop, T. M. Wheeler, F. Kallel, B. S. Garra, and T. Hall, "Elastic moduli of breast and prostate tissues under compression," *Ultrason. Imaging*, vol. 20 pp. 260-274, 1998.
7. M. O'Donnell, M. A. Lubinski, and S. Y. Emelianov, "Speckle tracking methods for ultrasonic elasticity imaging using short-time correlation," *IEEE Trans. Ultrason. Ferroelectr. Freq. Control*, vol. 46, no. 1, pp. 82-96, Jan. 1999.
8. T. Shiina, N. Nitta, E. Ueno, and J. C. Bamber, "Real time tissue elasticity imaging using the combined autocorrelation method," *J. Med. Ultrason.*, vol. 29, pp. 119-128, 2002.
9. A. Pesavento, C. Perrey, M. Krueger, and H. Ermert, "A time-efficient and accurate strain estimation concept for ultrasonic elastography using iterative phase zero estimation," *IEEE Trans. Ultrason. Ferroelectr. Freq. Control*, vol. 46, no. 5, pp. 1057-1067, Sept. 1999.
10. M. K. Jeong and S. J. Kwon, "Enhanced strain imaging using quality measure," *J. Acoust. Soc. Kor.*, vol. 27, no. 3E, pp. 84-94, Sept. 2008.
11. J. Ophir and I. Cespedes, "Reduction of image noise in elastography," *Ultrason. Imaging*, vol. 15, pp. 89-102, 1993.
12. J. Ophir and F. Kallel, "A least-squares strain estimator for elastography," *Ultrason. Imaging*, vol. 19, pp. 195-208, 1997.
13. S. Kaisar Alam, Jonathan Ophir, and E. E. Konofagou, "An adaptive strain estimator for elastography," *IEEE Trans. Ultrason. Ferroelectr. Freq. Control*, vol. 45, no. 2, pp. 461-472, Mar. 1998.
14. T. Varghese and J. Ophir, "Enhancement of echo-signal correlation in elastography using temporal stretching," *IEEE Trans. Ultrason. Ferroelectr. Freq. Control*, vol. 44, no. 1, pp. 173-180, Jan. 1997.
15. J. F. Lindop, G. M. Treece, A. H. Gee, and R. W. Prager, "Estimation of displacement location for enhanced strain imaging," *IEEE Trans. Ultrason. Ferroelectr. Freq. Control*, vol. 54, no. 9, pp. 1751-1771, Sept. 2007.
16. F. Kallel, J. Ophir, K. Magee, and T. Krouskop, "Elastographic imaging of low contrast elastic modulus distribution in tissue," *Ultrasound Med. Biol.*, vol. 24, no. 3, pp. 409-425, 1998.
17. R. Righetti, F. Kallel, R. J. Stafford, R. E. Price, T. A. Krouskop, J. D. Hazle, and J. Ophir, "Elastographic characterization of HIFU-induced lesions in canine livers", *Ultrasound Med. Biol.*, vol. 25, no. 7, pp. 1099-1113, 1999.
18. J. Ophir, S. K. Alam, B. Garra, F. Kallel, E. Konofagou, T. Krouskop, and T. Varghese, "Elastography: Ultrasonic estimation and imaging of the elastic properties of tissues," *J. Eng. Med.*, vol. 213, no. 3, pp. 203-233, 1999.
19. L. Sandrin, M. Tanter, S. Catheline, and M. Fink, "Shear modulus imaging with 2-D transient elastography," *IEEE Trans. Ultrason. Ferroelectr. Freq. Control*, vol. 49, no. 4, pp. 426-435, Apr. 2002.
20. M. Fink, L. Sandrin, M. Tanter, S. Catheline, S. Chaffai, J. Bercoff, and J. L. Gennisson, "Ultra high speed imaging of elasticity," in *Proc IEEE Ultrason. Symp.*, 2002, pp. 1811-1820.
21. K. J. Parker, L. Gao, S. K. Alam, D. Rubens, and R. M. Lerner, "Sonoelasticity Imaging: Theory and applications," in *Proc IEEE Ultrason. Symp.*, 1996, pp. 623-628.
22. L. S. Taylor, B. C. Porter, D. J. Rubens, and K. J. Parker, "Three dimensional sonoelastography: Principles and practices," *Phys. Med. Biol.*, vol. 45, pp. 1477-1494, 2000.
23. A. P. Sarvazyan, O. V. Rudenko, S. D. Swanson, J. B. Fowlkes, and S. Y. Emelianov, "Shear wave elasticity imaging: A new ultrasonic technology of medical diagnostics," *Ultrasound Med. Biol.*, vol. 24, no. 9, pp. 1419-1435, 1998.
24. S. McAleavey, M. Menon, and D. J. Rubens, "Acoustic radiation force impulse imaging of excised human prostates," in *Proc. IEEE*

Ultrason. Symp., 2000, pp. 1663–1666.
25. K. R. Nightingale, M. L. Palmeri, R. W. Nightingale, and G. E. Trahey, "On the feasibility of remote palpation using acoustic radiation force," *J. Acoust. Soc. Am.*, vol. 110, no. 1, pp. 625–634, July 2001.
26. K. Nightingale, M. S. Soo, R. Nightingale, E. Bentley, and G. Trahey, "In vivo demonstration of acoustic radiation force impulse imaging in the thyroid, abdomen, and breast," in *Proc. IEEE Ultrason. Symp.*, 2001, pp. 1633–1638.
27. K. Nightingale, M. S. Soo, R. Nightingale, R. Bentley, D. Stutz, M. Palmeri, J. Dahl, and G. Trahey, "Acoustic radiation force impulse imaging: Remote palpation of the mechanical properties of tissue," in *Proc. IEEE Ultrason. Symp.*, 2002, pp. 1821–1830.
28. B. J. Fahey, K. R. Nightingale, R. C. Nelson, M. L. Palmeri, and G. E. Trahey, "Acoustic radiation force impulse imaging of the abdomen: Demonstration of feasibility and utility," *Ultrasound Med. Biol.*, vol. 31, no. 9, pp. 1185–1198, 2005.
29. M. L. Palmeri, A. C. Sharma, R. R. Bouchard, R. W. Nightingale, and K. R. Nightingale, "A finite-element method model of soft tissue response to impulsive acoustic radiation force," *IEEE Trans. Ultrason. Ferroelectr. Freq. Control*, vol. 52, no. 10, pp. 1699–1712, Oct. 2005.
30. M. L. Palmeri, S. A. McAleavey, G. E. Trahey, and K. R. Nightingale, "Ultrasonic tracking of acoustic radiation force-induced displacements in homogeneous media," *IEEE Trans. Ultrason. Ferroelectr. Freq. Control*, vol. 53, no. 7, pp. 1300–1313, July 2006.
31. B. J. Fahey, R. C. Nelson, S. J. Hsu, D. P. Bradway, D. M. Dumont, and G. E. Trahey, "In vivo acoustic radiation force impulse imaging of abdominal lesions," in *Proc. IEEE Ultrason. Symp.*, 2007, pp. 440–443.
32. M. Fatemi and J. F. Greenleaf, "Ultrasound-stimulated vibro-acoustic spectrography," *Science*, vol. 280, no. 3, pp. 82–85, Apr. 1998.
33. M. Fatemi and J. F. Greenleaf, "Probing the dynamics of tissue at low frequencies with the radiation force of ultrasound," *Phys. Med. Biol.*, vol. 45, pp. 1449–1464, 2000.
34. J. Greenleaf, M. Fatemi, G. Silva, and M. Urban, "Vibro-acoustography: The most promising approaches and inferred needs for transducers and arrays," in *Proc. IEEE Ultrason. Symp.*, 2006, pp. 2372–2374.
35. A. Alizad, D. H. Whaley, R. R. Kinnick, J. F. Greenleaf, and M. Fatemi, "In vivo breast vibro-acoustography: Recent results and new challenges," in *Proc. IEEE Ultrason. Symp.*, 2006, pp. 1659–1662.
36. A. Alizad, D. H. Whaley, J. F. Greenleaf, and M. Fatemi, "Critical issues in breast imaging by vibro-acoustography," *Ultrasonics*, vol. 44, pp. 217–220, 2006.
37. J. Bercoff, M. Tanter, and M. Fink, "Supersonic shear imaging: A new technique for soft tissue elasticity mapping," *IEEE Trans. Ultrason. Ferroelectr. Freq. Control*, vol. 51, no. 4, pp. 396–409, Apr. 2004.
38. M. Tanter, J. Bercoff, A. Athanasiou, T. Deffieux, J.-L. Gennisson, G. Montaldo, M. Muller, A. Tardivon, and M. Fink, "Quantitative assessment of breast lesion viscoelasticity: Initial clinical results using supersonic shear imaging," *Ultrasound Med. Biol.*, vol. 34, no. 9, pp. 1373–1386, Sept. 2008.
39. J. Bercoff, A. Criton, C. C. Bacrie, J. Souquet, M. Tanter, J.-L. Gennisson, T. Deffieux, and M. Fink, "Shear wave elastography," in *Proc. IEEE Ultrason. Symp.*, 2008, pp. 321–324.
40. R. S. Lazebnik, "Tissue strain analytics: Virtual touch tissue imaging and quantification" [Online]. Available: http://www.medical.siemens.com/siemens/sv_SE/gg_us_FBAs/files/misc_downloads/Whitepaper_VirtualTouch.pdf.

[Profile]

• Mok-Kun Jeong

Mok-Kun Jeong received the B.S. degree in electrical engineering from Seoul National University in 1988, and the M.S. and Ph.D. degrees in electrical and electronic engineering from KAIST in 1990 and 1995, respectively. During the year 2000, he was a visiting researcher at the Department of Electrical and Computer Engineering, University of Minnesota, USA. Currently, he is a Professor of Electronic Engineering at Daejin University in Pocheon, Korea. His research interests are in medical ultrasound imaging systems.

• Sung-Jae Kwon

Sung-Jae Kwon received the B.S. degree in electronic engineering from Kyungpook National University in 1984, and the M.S. and Ph.D. degrees in electrical and electronic engineering from KAIST in 1986 and 1990, respectively. From 1990 to 1997 he was a principal researcher at Multimedia Laboratories, LG Electronics. Currently, he is a Professor of Communication Engineering at Daejin University in Pocheon, Korea. His research interests are in imaging, communication, broadcasting, and signal processing systems.